BACHELOR THESIS: Detailed Monte Carlo simulation of electron transport in a material slab

Adolfo Martín Baladrón
*Facultat de Física. Universitat de Barcelona. Diagonal 645, 08028 Barcelona, Spain.**

Advisor: Francesc Salvat
Facultat de Física (FQA and ICC). Universitat de Barcelona. Diagonal 645, 08028 Barcelona, Spain.

Abstract: A detailed Monte Carlo simulation of electron transport in a slab is performed by using a purely analytical interaction model. Elastic collisions are described by means of the differential cross section (DCS) obtained from the Born approximation with the Wentzel-Molière potential. Inelastic scattering is modelled on the basis of the Bethe formula for the stopping power with the Rao-Sahib and Wittry extrapolation to low energies. A simple model for the DCS of inelastic collisions is obtained by assuming the Thomson DCS for hard collisions and a "constant" DCS, separated by a cut-off determined from the equipartition rule. The model allows exact analytical random sampling from all the distributions involved in the process. Simulation results are compared with experimental data from the literature for electron beams with intermediate energies, from 9 keV to 100 keV energies. The agreement is qualitatively good, in spite of the simplicity of the model and the program.

I. INTRODUCTION

Radiation transport in matter has been a subject of intense interest since the beginning of the 20th century. High-energy charged particles penetrating matter suffer multiple interactions by which energy is transferred to the atoms and molecules of the material and secondary particles are produced.

For more than five decades, the Monte Carlo (MC) method has been used to describe the scattering and energy loss of charged particles penetrating matter[1]. The reliability of MC methods stems from their ability to incorporate realistic physical interaction models and atomic relaxation parameters and, also, from the ease with which they can handle complex geometries, thus making them well suited for the analysis of heterogeneous samples such as small particles, inclusion, interfaces or multilayer films. In a MC simulation, we are able not only to describe the penetration and slowing down of primary electrons, but the generation and transport of secondary radiation as well [2].

The reliability of MC simulation of multiple electron interactions is primarily determined by the accuracy of the adopted differential cross-section (DCS) models. A wide variety of MC models have been used in studies aimed at describing various aspects of the interaction of electron beams with solid specimens, including backscattering, secondary electron emission, x-ray emission and bremsstrahlung photon emission [3].

The motivation of this work was to learn the fundamentals of MC simulation of electron transport and to develop a computer program, called MCREL (based on a non-relativistic version of it), by using an interaction model where the DCSs of all interactions are described by simple expressions that allow the analytical random sampling of the transport quantities. The model is semi-relativistic and is applicable to electrons with kinetic energies up to about 500 keV, since bremsstrahlung emission and density-effect corrections (associated to the transverse interaction) are disregarded.

The material structure assumed in the simulation is a slab of a single element characterized by the atomic number Z and the density ρ (g/cm^3). The atomic density, *i.e.*, the number of atoms per unit volume, is

$$\mathcal{N} = \frac{N_{\rm A}\rho}{A_{\rm w}} \tag{1}$$

where N_A is the Avogadro number and $A_{\rm w}$ is the molar weight of the element.

II. ELASTIC SCATTERING

Elastic collisions of electrons (charge $-e$ and mass $m_{\rm e}$) with atoms of the element of atomic number Z are described by means of the DCS obtained from the Born approximation with the Wentzel [4] interaction potential

$$V(r) = \frac{Ze^2}{r}\,\exp(-r/R), \tag{2}$$

where

$$R = 0.88534 a_0 Z^{-1/3} \tag{3}$$

is the "screening radius", where

$$a_0 = \frac{\hbar}{m_{\rm e}e^2} \tag{4}$$

is the Bohr radius, being $\hbar$ the reduced Plank constant. This potential retains the familiar Thomas-Fermi scaling

*Electronic address: amartiba@gmail.com

of neutral atoms. The DCS for scattering of electrons with kinetic energy E by atoms of the element of atomic number Z that results from this model is

$$\frac{\mathrm{d}\sigma_{\mathrm{el}}}{\mathrm{d}\Omega} = \mathcal{C}\frac{1}{(2A+1-\cos\theta)^2} \tag{5}$$

where

$$\mathcal{C} = \left(\frac{Ze^2 m_e c^2}{(cp)^2}\right)^2 = \left(\frac{ZE_{\mathrm{h}} a_0 m_{\mathrm{e}} c^2}{E(E+2m_{\mathrm{e}}c^2)}\right)^2 \tag{6}$$

and

$$A = \frac{1}{4R^2k^2} = \frac{\hbar^2c^2}{4R^2(cp)^2}\,.$$

where c is the speed of light in vacuum, $E_{\mathrm{h}} = e^2/a_0$ is the Hartree energy, θ is the polar scattering angle and p is the (relativistic) momentum of the electron

$$cp = \sqrt{E(E+2m_{\mathrm{e}}c^2)}\,. \tag{7}$$

Molière [5] obtained a more realistic DCS by defining the "screening factor" A from calculations using a more elaborate (eikonal) approximation. In the simulations we use the Molière screening factor given by

$$A_{\mathrm{M}} = A\left(1.13 + 3.76\frac{\alpha Z(E+m_e c^2)^2}{E(E+2m_e c^2)}\right), \tag{8}$$

where $\alpha = e^2/(\hbar c)$ is the fine-structure constant.

The total cross section for elastic scattering is

$$\begin{aligned}\sigma_{\mathrm{el}} &= 2\pi\int_0^\pi \frac{\mathrm{d}\sigma_{\mathrm{el}}}{\mathrm{d}\Omega}\sin\theta\,\mathrm{d}\theta \\ &= \left(\frac{ZE_{\mathrm{h}}a_0 m_{\mathrm{e}}c^2}{E(E+2m_{\mathrm{e}}c^2)}\right)^2 \frac{\pi}{A_{\mathrm{M}}(A_{\mathrm{M}}+1)}\end{aligned} \tag{9}$$

The mean free path λ_{el} between elastic collisions is given by

$$\lambda_{\mathrm{el}}^{-1} = \mathcal{N}\sigma_{\mathrm{el}}. \tag{10}$$

Instead of the polar scattering angle θ, it is convenient to introduce the variable

$$\mu \equiv \frac{1-\cos\theta}{2} \tag{11}$$

and write the normalized probability distribution function (pdf) of the polar deflection as

$$p(\mu) = \frac{A_{\mathrm{M}}(A_{\mathrm{M}}+1)}{(A_{\mathrm{M}}+\mu)^2}. \tag{12}$$

This distribution is known as the Wentzel distribution. The inverse transform method yields the following sampling formula

$$\mu = \frac{A_{\mathrm{M}}\xi}{A_{\mathrm{M}}+1-\xi}\,, \tag{13}$$

where ξ is a random number uniformly distributed in (0,1). The azimuthal scattering angle ϕ is uniformly distributed between 0 and 2π, *i.e.*, $p(\phi) = 1/2\pi$. It is generated from the sampling formula

$$\phi = \xi\,2\pi. \tag{14}$$

III. INELASTIC COLLISIONS

Inelastic collisions of electrons moving with kinetic energy E in the material of atomic number Z are modelled on the basis of the Bethe formula for the stopping power (*i.e.*, average energy loss per unit path length), which reads

$$\frac{\mathrm{d}E}{\mathrm{d}s} = \mathcal{N}Z\frac{2\pi e^4}{m_{\mathrm{e}}v^2}\left[\ln\left(\frac{\mathrm{e}}{2}\frac{E^2}{I^2}\right) + f(\gamma)\right] \tag{15}$$

where v is the velocity of the electron, and

$$\gamma = \frac{E+m_{\mathrm{e}}c^2}{m_{\mathrm{e}}c^2}. \tag{16}$$

Notice that

$$v = \beta c = \sqrt{\frac{\gamma^2-1}{\gamma^2}}c, \tag{17}$$

where c is the speed of light in vacuum. The function $f(\gamma)$ represents the effect of relativity, and is given by [2]

$$f(\gamma) = \frac{1-(2\gamma-1)\ln(2)+\frac{1}{8}(\gamma-1)^2}{\gamma^2} + \ln(\gamma+1) - 1 \tag{18}$$

The parameter I is the so-called mean excitation energy, which completely characterizes the slowing down of charged particles in the medium. In the simulation program we use empirical I values recommended by the ICRU [6]. The formula

$$I = \begin{cases} 13.6Z \text{ eV} & \text{for } Z < 10 \\ (9.76 + 58.8Z^{-1.19})Z \text{ eV} & \text{for } Z \geq 10 \end{cases} \tag{19}$$

gives a rough approximation to the ICRU values.

For practical purposes, we write the Bethe formula as

$$\frac{\mathrm{d}E}{\mathrm{d}s} = C_{\mathrm{in}}\left[\ln\left(\frac{\mathrm{e}}{2}\frac{E^2}{I^2}\right) + f(\gamma)\right] \tag{20}$$

where $\mathrm{e} = 2.71828$ is the basis of natural logarithms and

$$C_{\mathrm{in}} \equiv \mathcal{N}Z\frac{2\pi e^2}{m_{\mathrm{e}}v^2} = 2\pi\mathcal{N}ZE_{\mathrm{h}}^2a_0^2\frac{\gamma^2}{(\gamma+1)E}. \tag{21}$$

This formula is valid only for energies much higher than I. As a matter of fact, for $E < (2/\mathrm{e})^{1/2}I$ it predicts a negative stopping power. To avoid negative losses we use the formula (20) only for energies higher than the energy where the Bethe expression has its inflexion point, $E_c = (2\mathrm{e}^3)^{1/2}I = 6.338\,I$. For energies lower than E_{c} we adopt the Rao-Sahib and Wittry [7] extrapolation

$$\frac{\mathrm{d}E}{\mathrm{d}s} = C_{\mathrm{in}}\left[2(2/\mathrm{e})^{3/4}\sqrt{\frac{E}{I}} + f(\gamma)\right] \tag{22}$$

which is more in accordance with the actual stopping power at low electron energies. The mean range (or continuous slowing down approximation range) of electrons with energy E is defined as

$$R = \int_0^E \left(\frac{\mathrm{d}E}{\mathrm{d}s}\right)^{-1} \mathrm{d}E. \tag{23}$$

To account for the discrete character of the interactions, and the associated straggling of the energy loss, we assume that hard collisions with large energy losses can be described as collisions with free electrons at rest. Accordingly, the DCS for these collisions is represented by the truncated Thomson DCS,

$$\frac{\mathrm{d}\sigma_{\mathrm{in,h}}}{\mathrm{d}W} = \frac{1}{\mathcal{N}} \frac{C_{\mathrm{in}}\gamma^2}{E(\gamma+1)} \frac{1}{W^2} \Theta(W - W_{\mathrm{cut}}) \Theta\left(\frac{E}{2} - W\right), \tag{24}$$

with the cut-off energy W_{cut} defined so that hard interactions contribute exactly half the stopping power given by the Bethe formula (as suggested by the equipartition rule [8]). After the collision we have two indistinguishable free electrons, and we consider that the projectile is the faster one. Consequently, the maximum allowed energy loss is $E/2$. That is, we require

$$\mathcal{N} \int_{W_{\mathrm{cut}}}^{E/2} W \frac{\mathrm{d}\sigma_{\mathrm{in,h}}}{\mathrm{d}W} \mathrm{d}W = \frac{1}{2} \frac{\mathrm{d}E}{\mathrm{d}s}, \tag{25}$$

which implies that

$$2 \ln\left(\frac{E}{2W_{\mathrm{cut}}}\right) = \begin{cases} 2(2/\mathrm{e})^{3/4} \sqrt{\dfrac{E}{I}} & \text{if } E \le E_{\mathrm{c}}, \\ \ln\left(\dfrac{\mathrm{e}}{2}\dfrac{E^2}{I^2}\right) & \text{otherwise.} \end{cases} \tag{26}$$

Thus, for energies higher than E_{c} we have

$$W_{\mathrm{cut}} = I/\sqrt{2\mathrm{e}}\,. \tag{27}$$

The contribution of the remaining (soft) interactions is described by assuming that the energy loss in each soft interaction is distributed uniformly in the interval from 0 to W_{cut}. The requirement that soft interactions contribute one half of the stopping power implies that

$$\frac{\mathrm{d}\sigma_{\mathrm{in,s}}}{\mathrm{d}W} = \frac{1}{W_{\mathrm{cut}}^2} \frac{1}{\mathcal{N}} \frac{\mathrm{d}E}{\mathrm{d}s} \Theta(W_{\mathrm{cut}} - W). \tag{28}$$

The integrated cross sections for hard and soft collisions are, respectively,

$$\sigma_{\mathrm{in,h}} = \int_{W_{\mathrm{cut}}}^{E/2} \frac{\mathrm{d}\sigma_{\mathrm{in,h}}}{\mathrm{d}W} \mathrm{d}W = \frac{1}{\mathcal{N}} C_{\mathrm{in}} \frac{E - 2W_{\mathrm{cut}}}{E W_{\mathrm{cut}}} \tag{29}$$

and

$$\sigma_{\mathrm{in,s}} = \int_0^{W_{\mathrm{cut}}} \frac{\mathrm{d}\sigma_{\mathrm{in,s}}}{\mathrm{d}W} \mathrm{d}W = \frac{1}{W_{\mathrm{cut}}} \frac{1}{\mathcal{N}} \frac{\mathrm{d}E}{\mathrm{d}s}\,. \tag{30}$$

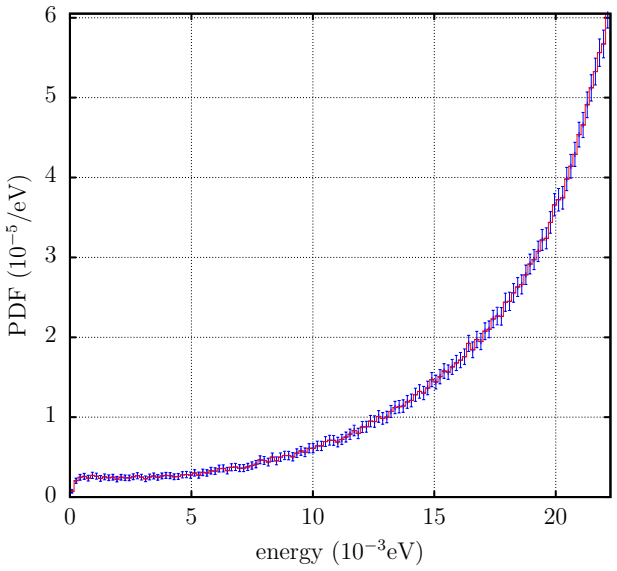

FIG. 1: Energy distribution of backscattered electrons, for gold with an initial energy $E_0 = 25\,\mathrm{keV}$, and mass thickness $\rho x = 1500\,\mu\mathrm{g/cm}^2$.

The mean free path λ_{in} between inelastic collisions is given by

$$\begin{aligned} \lambda_{\mathrm{in}}^{-1} &= \mathcal{N}\,(\sigma_{\mathrm{in,h}} + \sigma_{\mathrm{in,h}}) \\ &= C_{\mathrm{in}} \frac{E - 2W_{\mathrm{cut}}}{W_{\mathrm{cut}}} + \frac{1}{W_{\mathrm{cut}}} \frac{\mathrm{d}E}{\mathrm{d}s} \end{aligned} \tag{31}$$

In the simulation the kind of each inelastic collision is selected randomly according to the respective total cross sections. The pdf of the energy loss W in a single hard interaction is

$$p(W) = \frac{E W_{\mathrm{cut}}}{E - 2W_{\mathrm{cut}}} \frac{1}{W^2}, \qquad W \in (W_{\mathrm{cut}}, E/2). \tag{32}$$

and the pdf of W in soft interactions is uniform in $(0, W_{\mathrm{cut}})$. The inverse transform method yields the sampling formulas

$$W = \begin{cases} \dfrac{E W_{\mathrm{cut}}}{E - \xi(E - 2W_{\mathrm{cut}})} & \text{for hard interactions,} \\ \xi W_{\mathrm{cut}} & \text{for soft interactions,} \end{cases} \tag{33}$$

We disregard the small angular deflections due soft interactions. For hard interactions the polar scattering angle is obtained from the kinematics of non-relativistic binary collisions with free electrons at rest, that is

$$\cos\theta = \sqrt{1 - \frac{W}{E}}. \tag{34}$$

Again, the azimuthal angle ϕ is uniformly distributed between 0 and 2π,

$$\phi = \xi\, 2\pi. \tag{35}$$

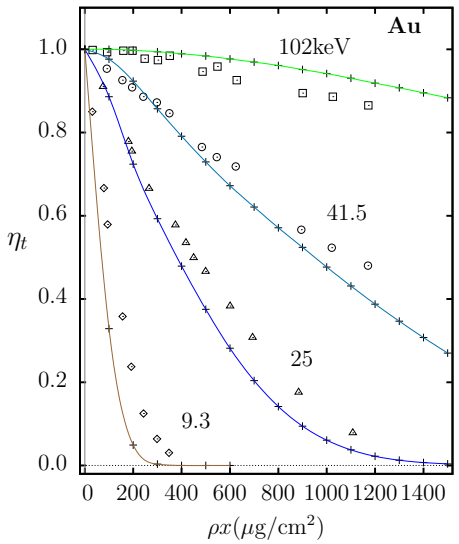

FIG. 2: Transmission fraction, η_t, for electrons with the indicated kinetic energies, through gold films, as a function of mass thickness ρx. Crosses (joined by solid lines for visual aid) show MCREL results. Symbols are experimental results from Reimer and Drescher [9] (rhombuses, circles and squares) and Neubert and Rogaschewski [10] (triangles).

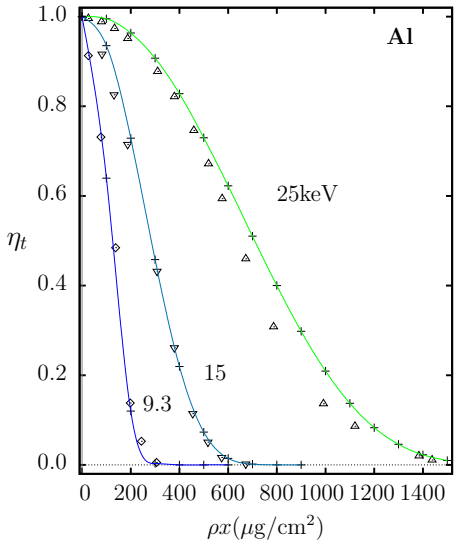

FIG. 3: Transmission fraction, η_t, for electrons with the indicated kinetic energies, through aluminium films, as a function of mass thickness ρx. Crosses (joined by solid lines for visual aid) show MCREL results. Symbols are experimental results from Reimer and Drescher [9] (rhombuses) and Neubert and Rogaschewski [10] (triangles).

We consider that secondary electrons are emitted in hard interactions with initial energy $E_{\rm sec} = W - W_{\rm cut}$ and direction in the scattering plane (defined by the initial and final momenta of the projectile) forming an angle of 90 degrees with the direction of the primary. That is, the direction of the secondary electron corresponds to "scattering angles" $\theta_{\rm sec}$ and $\phi_{\rm sec}$ given by

$$\cos\theta_{\rm sec} = \sqrt{W/E} \qquad \text{and} \qquad \phi_{\rm sec} = \phi + \pi. \tag{36}$$

IV. TRACKING ALGORITHM

The inverse mean free path between interactions is

$$\lambda^{-1} = \lambda_{\rm el}^{-1} + \lambda_{\rm el}^{-1} \tag{37}$$

The distance s to the next interaction is sampled from the familiar exponential distribution

$$s = -\lambda \ln(\xi) \tag{38}$$

The kind of interaction is determined from the probabilities

$$p_{\rm el} = \lambda_{\rm el}^{-1}/\lambda^{-1}, \qquad p_{\rm in} = \lambda_{\rm in}^{-1}/\lambda^{-1}. \tag{39}$$

After sampling the interaction variables, we change the energy and direction of motion of the electron, and we iterate the process until either the electron leaves the foil, or its energy becomes less than the absorption energy $E_{\rm abs}$, which is set to 100 keV.

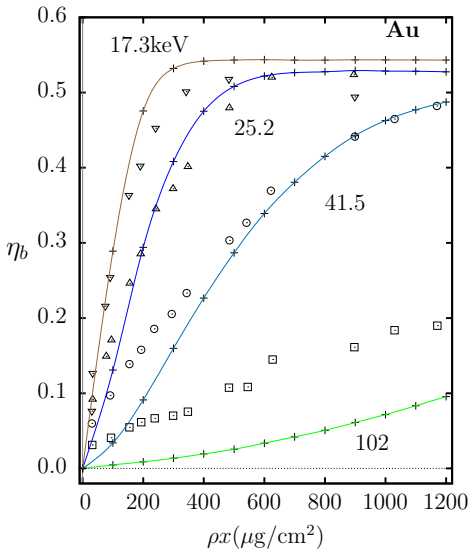

FIG. 4: Backscattered fraction, η_b, for electrons with the indicated kinetic energies, through gold films, as a function of mass thickness ρx. Crosses (joined by solid lines for visual aid) show MCREL results. Symbols are experimental results from Reimer and Drescher [9]

The program allows the use of an initial Gaussian energy distribution, setting its mean energy and standard deviation. Even so, in all simulations the latter is set to zero. We have therefore a simulation for electrons with an initial energy E_0(eV) and a material slab of thickness x(cm).

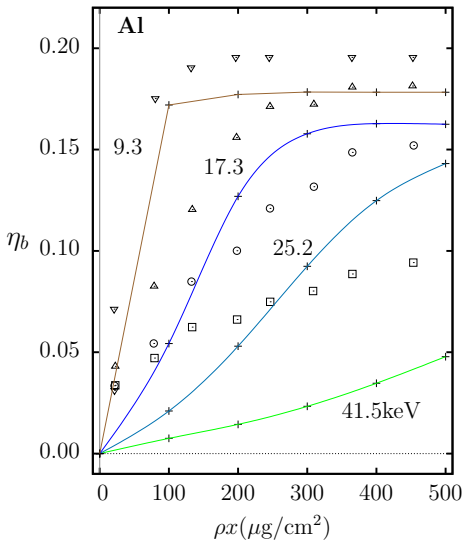

FIG. 5: Backscattered fraction, η_b, for electrons with the indicated kinetic energies, through aluminium films, as a function of mass thickness ρx. Crosses (joined by solid lines for visual aid) show MCREL results. Symbols are experimental results from Reimer and Drescher [9]

V. COMPARISON WITH EXPERIMENTAL DATA

The number of random electron tracks generated in each simulation run was 10^6. To illustrate the kind of information provided by the code, figure 1 shows an example of calculated energy distribution of electrons backscattered in gold. The relative statistical uncertainties of the results shown in figures 2 to 5 is less than 1%.

The transmission fraction, η_t, is the fraction of electrons crossing the whole thickness of the foil. This number is affected by the absorption energy, $E_{\rm abs}$, adopted in the simulations, *i.e.*, only electrons with final energy greater than $E_{\rm abs}$ are counted. Figure 2 shows the transmitted fraction for electron beams with different initial kinetic energies through gold films, as a function of the film mass thickness ρx, where ρ is the density of the material in μg/cm^3 and x is the linear thickness of the film in cm. Simulation results are closer to experimental data for intermediate energies over the studied range. This behaviour is also found for smaller atomic numbers Z, as we can see on figure 3 for aluminium.

The backscattered fraction is the fraction of electrons coming back towards the initial electron beam. In figures 4 and 5 the backscattered fraction is represented as a function of mass thickness for gold and aluminium. The relative differences between the simulations and the experiments are seen to increase when the energy of the beam decreases.

VI. CONCLUSIONS

Comparison of simulation results with the considered experimental measurements, [9][10], shows that the computer program MCREL provides a qualitatively realistic description of the penetration and energy loss of electrons in material slabs, over intermediate energies among the considered range, despite the simplicity of the model and the program. MCREL gives a reasonable first approximation to the solution of the modelled problem.

Acknowledgments

I wish to deeply express my gratitude to my advisor Francesc Salvat, for his patience, dedication and commitment, and for his wise guidance and mentoring, and to my partner Elisenda Mantilla, for her tireless support and unconditional love.

[1] M. J. Berger, in *Methods in Computational Physics*, edited by B. Alder, S. Fernbach, and M. Rotenberg (Academic Press, New York, 1963), vol. 1, pp. 135–215.

[2] F. Salvat, PENELOPE-*2014: A code System for Monte Carlo Simulation of Electron and Photon Transport* (OECD/NEA Data Bank, NEA/NSC/DOC(2015)3, Issy-les-Moulineaux, France, 2015), available from `http://www.nea.fr/lists/penelope.html`.

[3] A. Eades, Microscopy Research and Technique **35**, 413 (1996), ISSN 1097-0029, URL `http://dx.doi.org/10.1002/1097-0029(19961201)35:5<413::AID-JEMT1070350502>3.0.CO;2-6`.

[4] G. Wentzel, Z. Phys. **42**, 590 (1927).

[5] G. Molière, Z. Naturforsch. **2a**, 133 (1947).

[6] ICRU Report 85, *Fundamental Quantities and Units for Ionizing Radiation* (ICRU, Bethesda, MD, 2011).

[7] T. S. RaoSahib and D. B. Wittry, Journal of Applied Physics **45**, 5060 (1974), https://doi.org/10.1063/1.1663184, URL `https://doi.org/10.1063/1.1663184`.

[8] J. Lindhard and A. Winther, Mat. Fys. Medd. Dan. Vid. Selsk. **34**, 1 (1964).

[9] L. Reimer and H. Drescher, J. Phys. D: Appl. Phys. **10**, 805 (1977), URL `http://stacks.iop.org/0022-3727/10/i=5/a=022`.

[10] G. Neubert and S. Rogaschewski, Journal of Physics D Applied Physics **17**, 2439 (1984).